

Thermodynamics of $(2 + 1)$ -flavor QCD: Confronting Models with Lattice Studies

B.-J. Schaefer,^{1,*} M. Wagner,^{2,3,†} and J. Wambach^{2,4}

¹*Institut für Physik, Karl-Franzens-Universität, A-8010 Graz, Austria*

²*Institut für Kernphysik, TU Darmstadt, D-64289 Darmstadt, Germany*

³*ExtreMe Matter Institute EMMI, GSI Helmholtzzentrum für Schwerionenforschung GmbH, D-64291 Darmstadt, Germany*

⁴*Gesellschaft für Schwerionenforschung GSI, D-64291 Darmstadt, Germany*

The Polyakov-quark-meson (PQM) model, which combines chiral as well as deconfinement aspects of strongly interacting matter is introduced for three light quark flavors. An analysis of the chiral and deconfinement phase transition of the model and its thermodynamics at finite temperatures is given. Three different forms of the effective Polyakov loop potential are considered. The findings of the $2 + 1$ flavor model investigations are confronted to corresponding recent QCD lattice simulations of the RBC-Bielefeld, HotQCD and Wuppertal-Budapest collaborations. The influence of the heavier quark masses, which are used in the lattice calculations, is taken into account. In the transition region the bulk thermodynamics of the PQM model agrees well with the lattice data.

PACS numbers: 12.38.Aw, 11.10.Wx, 11.30.Rd, 12.38.Gc

I. INTRODUCTION

While the underlying microscopic theory of the strong interaction, Quantum Chromodynamics (QCD), is known for several decades, our knowledge on its phase structure under extreme conditions is still rather limited [1, 2]. Understanding its critical properties and phase transitions is a major focus which is addressed in both theoretical and experimental studies. Heavy-ion collisions in such experiments at the highest currently available energies are surprisingly well-described by ideal relativistic hydrodynamics (see e.g. [3] and references therein). This demands a detailed knowledge of the bulk thermodynamics and the equation of state of strongly-interacting matter.

Different regimes of the QCD phase diagram can be examined by employing various theoretical methods. For example, lattice QCD simulations (see e.g. [4]) are applicable to the finite temperature regime of the phase diagram but at finite chemical potentials the fermion sign problem is still a considerable obstacle. At finite temperatures recent lattice calculations describe the QCD thermodynamics reliably since larger volumes are used and the quark masses are closer to their physical values. Although most lattice simulations for $(2 + 1)$ -flavor QCD agree that chiral symmetry is restored by a smooth crossover transition [5] there is still an ongoing discussion concerning the (pseudo)critical temperatures of the chiral and deconfinement transition [6]. One group (RBC-Bielefeld, HotQCD) sees a coincidence of both transitions [7, 8] while the Wuppertal-Budapest group finds a larger deconfinement temperature compared to the chiral one by examining the peaks of the chiral and Polyakov-loop susceptibilities [9, 10].

Effective NJL-type models can address chiral aspects

of the QCD phase diagram and do not suffer from limitations at finite chemical potentials. It is expected that the critical behavior of such models is governed by the same universality class as QCD [11]. But, due to the lack of confinement, they fail in describing the thermodynamics of strongly interacting matter, in particular the deconfinement transition. However, both transitions become accessible with extended NJL-type models which are augmented with the Polyakov loop. Recently, most studies in these Polyakov-loop NJL-type models (PNJL) focus on two quark flavors with an effective polynomial or logarithmic Polyakov loop potential [12–21]. The thermodynamics of these models has often been compared to older two-flavor lattice data with large quark masses (e.g. [22]) while in the model calculations physical values have been used. Recent $(2 + 1)$ -flavor studies in the PNJL [23–27] or Polyakov-quark-meson (PQM) models [28–30] indeed agree better with the corresponding lattice data although the used quark masses still differ.

Much progress has been achieved in lattice studies for $(2+1)$ -flavor QCD thermodynamics, e.g. [7, 8, 10, 31–34]. In this work a $(2 + 1)$ -flavor PQM model study is compared with the most recent lattice data of the HotQCD and RBC-Bielefeld [8, 32] and the Wuppertal-Budapest (WB) collaborations [10]. In the lattice simulations of the HotQCD and RBC-Bielefeld collaborations a ratio of the physical strange quark mass to the light one of 10 is typically used which yields too large light quark masses. These quark masses entail a pion mass of $m_\pi \sim 220$ MeV and a kaon mass of $m_K \sim 500$ MeV using improved staggered fermions (p4 and asqtad actions). They observe a coincidence of the chiral and the deconfinement transition around temperatures $T \sim 185 - 195$ MeV. Coinciding temperatures result also in a two flavor QCD analysis if quantum fluctuations are incorporated, see e.g. [35, 36].

For the chiral order parameter and the strange quark number susceptibility we also compare our results with lattice data from the Wuppertal-Budapest collaboration which they have obtained for physical quark masses on $N_\tau = 10$ lattices [10]. In contrast to the other lattice col-

*E-Mail:bernd-jochen.schaefer@uni-graz.at

†E-Mail:mathias.wagner@physik.tu-darmstadt.de

laborations they find a chiral transition at temperatures lower than the one for the deconfinement transition, i.e., $T_\chi \sim 146 \text{ MeV} < T_d \sim 170 \text{ MeV}$.

The outline of this work is as follows: after introducing the PQM model for $N_f = 2 + 1$ quark flavors, the implementation of various effective Polyakov-loop potentials is discussed. The thermodynamic potential of the PQM model in mean-field approximation is derived in Sec. III. The resulting chiral and confinement/deconfinement phase structure and its dependence on the model parameters and various Polyakov-loop potentials are presented in Sec. IV. A detailed comparison for several thermodynamic quantities such as the equation of state and various susceptibilities with lattice data is carried out in Sec. V. Here, the effect of the heavier pion masses and different Polyakov loop potential choices is explicitly considered. Finally, conclusions are drawn in Sec. VI.

II. POLYAKOV-QUARK-MESON MODEL

In order to address the linkage between the chiral symmetry restoration and aspects of the confinement/deconfinement transition we introduce the Polyakov-quark-meson (PQM) model for three quark flavors. It is a straightforward generalization of the two quark flavor model [36] and is a combination of the chiral linear σ -model [37] with the Polyakov loop $\Phi(\vec{x})$, the thermal expectation value of a color traced Wilson loop in the temporal direction

$$\Phi(\vec{x}) = \frac{1}{N_c} \langle \text{tr}_c \mathcal{P}(\vec{x}) \rangle. \quad (1)$$

The matrix-valued Polyakov loop operator $\mathcal{P}(\vec{x})$ in the fundamental representation of the $SU(N_c)$ gauge group contains the temporal vector field A_0 ,

$$\mathcal{P}(\vec{x}) = \text{P exp} \left(i \int_0^\beta d\tau A_0(\vec{x}, \tau) \right), \quad (2)$$

where P denotes path ordering and $\beta = 1/T$ the inverse temperature [38]. Since the Polyakov loop in this model is used as a classical variable, implementation details in Eq. (2) are not important in the present work.

The expectation value Eq. (1) serves as an order parameter of the center symmetry in the heavy quark mass limit: it is finite when the center symmetry is spontaneously broken and vanishes for center-symmetric states. Hence, Φ is finite at high temperatures corresponding to the deconfined plasma phase and it vanishes at low temperatures in the confined, center-symmetric phase. However, in a system with dynamical quarks the center symmetry is always broken but Φ still seems to be a good indicator of the confinement/deconfinement transition. Therefore, we regard Φ as an approximate order parameter for this phase transition.

The PQM Lagrangian consists of a quark-meson contribution and a Polyakov-loop potential $\mathcal{U}(\Phi[A], \bar{\Phi}[A])$, which depends on the Polyakov-loop variable Φ and its hermitian conjugate $\bar{\Phi} = \langle \text{tr}_c \mathcal{P}^\dagger \rangle / N_c$. The coupling of the uniform temporal background gauge field to the quarks is achieved by replacing the standard derivative ∂_μ in the quark-meson contribution by a covariant derivative

$$D_\mu = \partial_\mu - i A_\mu, \quad A_\mu = \delta_{\mu 0} A^0 \quad (3)$$

where the $SU(N_c)$ gauge coupling g_s is included in $A_\mu = g_s A_\mu^a \lambda^a / 2$. The usual Gell-Mann matrices are denoted by λ^a with $a = 1, \dots, N_c^2 - 1$. This leads to the Lagrangian

$$\mathcal{L}_{\text{PQM}} = \bar{q} (i \not{D} - g \phi_5) q + \mathcal{L}_m - \mathcal{U}(\Phi[A], \bar{\Phi}[A]), \quad (4)$$

where the column vector $q = (u, d, s)$ denotes the quark field for $N_f = 3$ flavors and $N_c = 3$ color degrees of freedom. For three quark flavors the interaction between the quarks and the meson nonets is implemented by a flavor-blind Yukawa coupling g and the meson matrix

$$\phi_5 = T_a (\sigma_a + i \gamma_5 \pi_a), \quad (5)$$

where the $T_a = \lambda_a / 2$, $a = 0, \dots, 8$ are the nine generators of the $U(3)$ symmetry with $\lambda_0 = \sqrt{\frac{2}{3}} \mathbf{1}$. The generators T_a are normalized to $\text{Tr}(T_a T_b) = \delta_{ab} / 2$ and obey the $U(3)$ algebra $[T_a, T_b] = i f_{abc} T_c$ and $\{T_a, T_b\} = d_{abc} T_c$ respectively with the corresponding standard symmetric d_{abc} and antisymmetric f_{abc} structure constants of the $SU(3)$ group and

$$f_{ab0} = 0, \quad d_{ab0} = \sqrt{\frac{2}{3}} \delta_{ab}. \quad (6)$$

The nine scalar ($J^P = 0^+$) mesons are labeled by the σ_a fields and accordingly the nine pseudoscalar ($J^P = 0^-$) mesons by the π_a fields.

The remaining, purely mesonic contribution reads

$$\begin{aligned} \mathcal{L}_m = & \text{Tr} (\partial_\mu \phi^\dagger \partial^\mu \phi) - m^2 \text{Tr} (\phi^\dagger \phi) - \lambda_1 [\text{Tr} (\phi^\dagger \phi)]^2 \\ & - \lambda_2 \text{Tr} (\phi^\dagger \phi)^2 + c (\det(\phi) + \det(\phi^\dagger)) \\ & + \text{Tr} [H(\phi + \phi^\dagger)], \end{aligned} \quad (7)$$

with the abbreviation

$$\phi = T_a \phi_a = T_a (\sigma_a + i \pi_a), \quad (8)$$

representing a complex (3×3) -matrix for $N_f = 3$.

Chiral symmetry is broken explicitly by the last term in Eq. (7) where

$$H = T_a h_a \quad (9)$$

is a again (3×3) -matrix with nine external parameters h_a . The $U(1)_A$ -symmetry is explicitly broken by the 't Hooft determinant term with a constant strength c . Further

details concerning the three-flavor quark-meson part of the PQM model can be found in [39].

The final form of the effective gluon field potential \mathcal{U} in Eq. (4) is constructed in terms of the Polyakov loop variables Φ and $\bar{\Phi}$. It preserves the center symmetry of the pure Yang-Mills (YM) theory [40, 41]. However, several explicit choices of the Polyakov loop potential are possible which we collect in the following.

A. Polyakov loop potentials

The functional form of the Polyakov loop potential is motivated by the underlying QCD symmetries in the pure gauge limit, i.e. for infinitely heavy quarks. The different parameterizations reproduce a first-order transition at $T \sim 270$ MeV in the pure gauge sector for $N_c = 3$ [13, 14, 25].

The simplest choice is based on a Ginzburg-Landau ansatz [13, 36]. The underlying $Z(3)$ center symmetry is broken spontaneously in the pure Yang-Mills case which should be respected by the ansatz. Hence, an expansion in terms of the order parameter results in

$$\frac{\mathcal{U}_{\text{poly}}}{T^4} = -\frac{b_2}{4} (|\Phi|^2 + |\bar{\Phi}|^2) - \frac{b_3}{6} (\Phi^3 + \bar{\Phi}^3) + \frac{b_4}{16} (|\Phi|^2 + |\bar{\Phi}|^2)^2 \quad (10)$$

with a temperature-dependent coefficient

$$b_2(T) = a_0 + a_1 \left(\frac{T_0}{T}\right) + a_2 \left(\frac{T_0}{T}\right)^2 + a_3 \left(\frac{T_0}{T}\right)^3. \quad (11)$$

The cubic Φ terms in Eq. (10) are required to break the $U(1)$ symmetry of the remaining terms down to $Z(3)$. The potential parameters are adjusted to the pure gauge lattice data such that the equation of state and the Polyakov loop expectation values are reproduced. This yields the following set of parameters [13]:

$$a_0 = 6.75, \quad a_1 = -1.95, \quad a_2 = 2.625, \quad a_3 = -7.44 \\ b_3 = 0.75, \quad b_4 = 7.5.$$

The parameter $T_0 = 270$ MeV corresponds to the transition temperature in the pure YM theory. The extension of the potential Eq. (10) to finite chemical potential and the remaining ambiguity is discussed in [36]. At vanishing chemical potential the constraint $\bar{\Phi} = \Phi^\dagger$ is still valid and the potential corresponds to a polynomial expansion in Φ and $\bar{\Phi}$, including the product term $\Phi\bar{\Phi}$ as in Refs. [40, 42].

An improved ansatz [14] results in

$$\frac{\mathcal{U}_{\text{log}}}{T^4} = -\frac{1}{2} a(T) \bar{\Phi} \Phi + b(T) \ln \left[1 - 6\bar{\Phi}\Phi + 4(\Phi^3 + \bar{\Phi}^3) - 3(\bar{\Phi}\Phi)^2 \right] \quad (12)$$

with the temperature-dependent coefficients

$$a(T) = a_0 + a_1 \left(\frac{T_0}{T}\right) + a_2 \left(\frac{T_0}{T}\right)^2 \quad (13)$$

and

$$b(T) = b_3 \left(\frac{T_0}{T}\right)^3. \quad (14)$$

Here, the logarithmic form constrains Φ and $\bar{\Phi}$ to values smaller than one, in contrast to the polynomial potential ansatz.

Again, the parameters of Eq. (12) are fitted to the pure gauge lattice data, resulting in [14]

$$a_0 = 3.51, \quad a_1 = -2.47, \quad a_2 = 15.2, \quad b_3 = -1.75 \quad (15)$$

Both fits reproduce equally well the equation of state and the Polyakov loop expectation value.

A third version, proposed by Fukushima [25], is inspired by a strong-coupling analysis

$$\frac{\mathcal{U}_{\text{Fuku}}}{T^4} = -\frac{b}{T^3} \left[54e^{-a/T} \Phi \bar{\Phi} + \ln(1 - 6\Phi\bar{\Phi} - 3(\Phi\bar{\Phi})^2 + 4(\Phi^3 + \bar{\Phi}^3)) \right] \quad (16)$$

and has only two parameters a and b . The first term is reminiscent of the nearest-neighbor interaction and the logarithmic term is again due to the Haar measure as in (12). The parameter a determines the deconfinement transition, i.e., the transition temperature in pure gauge theory, while b controls the mixing of the chiral and the deconfinement transition. In this version, the parameters are not fitted to lattice data but they reproduce a first-order transition at $T_0 \sim 270$ MeV in the pure gauge sector for

$$a = 664 \text{ MeV}, \quad b = (196.2 \text{ MeV})^3. \quad (17)$$

In a mean-field PNJL analysis with this potential ansatz a coincidence of the chiral and deconfinement transitions at $T_c \sim 200$ MeV for vanishing chemical potential is found [25].

Another significant difference of the last potential ansatz is visible in the thermodynamic pressure at high temperatures. In this case, both the unconfined transverse gluons as well as the Polyakov loop which corresponds to longitudinal gluons contribute to the pressure. But since the Polyakov loop potentials are fitted to pure gauge lattice data, they thus reproduce the pressure of both the longitudinal and the transverse gluons and might therefore overcount the degrees of freedom in the chirally symmetric phase. However, the potential ansatz by Fukushima excludes these transverse gluon contributions at high temperatures. This difference will become important when thermodynamic quantities, obtained with various Polyakov loop potentials, are compared to lattice data. However, for temperatures

N_f	0	1	2	2+1	3
T_0 [MeV]	270	240	208	187	178

TABLE I: The critical temperature T_0 for N_f massless flavors according to [36]. The value for 2 + 1 flavors has been estimated by using HTL/HDL theory for a massive strange quark with $m_s = 150$ MeV.

$T \lesssim 1.5T_0$ the deviations of the Polyakov loop potentials to the pressure are negligible.

In the presence of dynamical quarks, the running coupling of QCD is modified by fermionic contributions. The size of this effect can be estimated within perturbation theory, see e.g. [43]. This leads to an N_f -dependent modification of the expansion coefficients in the polynomial Polyakov loop potential. The effect can be mapped onto an N_f -dependent T_0 resulting in Tab. I [36]. Similar to [43], the critical temperature T_0 decreases for increasing N_f .

In this work the T_0 -dependence on the phase structure will also be investigated for the logarithmic and polynomial potential.

III. THERMODYNAMIC POTENTIAL

In order to investigate the phase structure of the PQM model the thermodynamic potential is evaluated in mean-field approximation similar to [36, 39]. In the derivation we will consider the dependence on the temperature and three quark chemical potentials, μ_f , one for each flavor f . However, in the isospin-symmetric case the light masses are degenerated, i.e. $m_l \equiv m_u = m_d$ and

the thermodynamic potential depends only on two independent quark chemical potentials, $\mu_l = (\mu_u + \mu_d)/2$ and μ_s . Note, that the quark chemical potential μ_q is simply related to the baryochemical potential μ_B by $\mu_q = \mu_B/3$ with $\mu_B = 2\mu_l + \mu_s$. Thus, only two order parameters σ_0 and σ_8 emerge in the singlet-octet basis. In the following these condensates are rotated to the non-strange (σ_x) and strange (σ_y) basis, see [39] for details.

In mean-field approximation the thermodynamic potential consists of the mesonic $U(\sigma_x, \sigma_y)$, the quark/antiquark $\Omega_{\bar{q}q}$ and the Polyakov loop contributions

$$\Omega = U(\sigma_x, \sigma_y) + \Omega_{\bar{q}q}(\sigma_x, \sigma_y, \Phi, \bar{\Phi}) + \mathcal{U}(\Phi, \bar{\Phi}) . \quad (18)$$

Explicitly, the mesonic contribution reads

$$U(\sigma_x, \sigma_y) = \frac{m^2}{2} (\sigma_x^2 + \sigma_y^2) - h_x \sigma_x - h_y \sigma_y - \frac{c}{2\sqrt{2}} \sigma_x^2 \sigma_y^2 + \frac{\lambda_1}{2} \sigma_x^2 \sigma_y^2 + \frac{1}{8} (2\lambda_1 + \lambda_2) \sigma_x^4 + \frac{1}{8} (2\lambda_1 + 2\lambda_2) \sigma_y^4 , \quad (19)$$

and has six parameters $m^2, c, \lambda_1, \lambda_2, h_x, h_y$. They are fitted to well-known pseudoscalar meson masses $m_\pi, m_K, m_\eta^2 + m_{\eta'}^2$ and two weak-decay constants f_π, f_K . The mass of the scalar σ meson, m_σ , is used to complete the fit. Since the experimental situation concerning this resonance, cf. [44] is not clear we vary m_σ from 500 MeV to 800 MeV which results in different parameter sets, see also [39].

The Polyakov loop variables are coupled to the fermionic part via

$$\Omega_{\bar{q}q}(\sigma_x, \sigma_y, \Phi, \bar{\Phi}) = -2T \sum_{f=u,d,s} \int \frac{d^3p}{(2\pi)^3} \left\{ \ln \left[1 + 3(\Phi + \bar{\Phi} e^{-(E_{q,f} - \mu_f)/T}) e^{-(E_{q,f} - \mu_f)/T} + e^{-3(E_{q,f} - \mu_f)/T} \right] + \ln \left[1 + 3(\bar{\Phi} + \Phi e^{-(E_{q,f} + \mu_f)/T}) e^{-(E_{q,f} + \mu_f)/T} + e^{-3(E_{q,f} + \mu_f)/T} \right] \right\} . \quad (20)$$

The flavor-dependent single-particle energies are given by

$$E_{q,f} = \sqrt{k^2 + m_f^2} \quad (21)$$

with the flavor-dependent quark masses

$$m_l = g\sigma_x/2 \quad \text{and} \quad m_s = g\sigma_y/\sqrt{2} \quad (22)$$

for the light and strange quarks, respectively. The Yukawa coupling g is fixed to reproduce a light constituent quark mass of $m_q \approx 300$ MeV. This in turn predicts a strange constituent quark mass of $m_s \approx 433$ MeV. From Eq. (20) one recognizes the suppressions of single-quark contributions in the hadronic phase where

$\bar{\Phi}, \Phi \sim 0$ while baryon-like objects, which are composites of $N_c = 3$ quarks, contribute to the potential. In this way some confinement properties are mimicked in this model in a statistical sense. On the other hand, for $\bar{\Phi}, \Phi \sim 1$, the Polyakov loop modifications decouple from the fermionic part and Eq. (20) turns to the usual quark/antiquark contribution of the pure quark-meson model [39].

Finally, the temperature- and quark chemical potential dependence of the four order parameters for the chiral and deconfinement transition are determined as solutions of the corresponding equations of motion. These coupled equations are obtained by minimizing the grand potential, Eq. (18), with respect to the four constant mean-

fields $\langle\sigma\rangle_x$, $\langle\sigma\rangle_y$, $\langle\Phi\rangle$ and $\langle\bar{\Phi}\rangle$:

$$\frac{\partial\Omega}{\partial\sigma_x} = \frac{\partial\Omega}{\partial\sigma_y} = \frac{\partial\Omega}{\partial\Phi} = \frac{\partial\Omega}{\partial\bar{\Phi}} \Big|_{\min} = 0, \quad (23)$$

where $\min = (\sigma_x = \langle\sigma_x\rangle, \sigma_y = \langle\sigma_y\rangle, \Phi = \langle\Phi\rangle, \bar{\Phi} = \langle\bar{\Phi}\rangle)$ labels the global minimum.

IV. FINITE-TEMPERATURE PHASE TRANSITIONS

The (pseudo)critical temperatures for the various transitions are determined as the inflection point of the corresponding order parameters. The resulting critical temperatures at vanishing chemical potentials for the non-strange T_χ and strange chiral transitions T_χ^s as well as for the deconfinement transition T_d for three different Polyakov loop potentials and various combinations of m_σ and T_0 are summarized in Tab. II.

In general, the inclusion of the Polyakov loop shifts the (non-strange) chiral transition at vanishing quark chemical potential, $\mu_q = 0$, to higher temperatures. In addition, m_σ and T_0 affect the chiral and deconfinement transition temperatures and their interplay as follows: larger values of m_σ and T_0 shift again the transition to higher temperatures. A similar trend concerning the m_σ -sensitivity on the phase structure was observed in a pure three flavor quark-meson model [39].

For the chosen parameter sets we find $T_\chi \geq T_d$. This behavior is expected since the Polyakov loop suppresses fermionic contributions to the thermodynamic potential in the confined phase. However, these contributions drive the chiral phase transition and thus a delayed deconfinement transition always delays the chiral symmetry restoration. This becomes most obvious for small values of $m_\sigma \approx 500 - 600$ MeV, where the chiral transition occurs in the pure QM model already at $T_\chi \lesssim 150$ MeV. As a consequence, the PQM model cannot reproduce the Wuppertal-Budapest scenario [9, 10] with $T_\chi \ll T_d \approx T_\chi^s$. Only for the polynomial Polyakov loop potential with the extreme parameters $T_0 = 270$ MeV and $m_\sigma = 500$ MeV the case $T_\chi < T_d$ is seen. However, the deconfinement transition is a very smooth crossover and overlaps with the chiral transition.

For the logarithmic and Fukushima potential only few parameter sets ($m_\sigma = 500$ MeV and 600 MeV) are found where both transitions coincide. Even in the deconfined phase the quark contribution to the thermodynamic potential is not sufficiently large to restore chiral symmetry immediately and thus $T_\chi > T_d$ is obtained.

In the following we choose a parameter set where both transitions coincide at $\mu_q = 0$ as suggested by the RBC-Bielefeld and HotQCD lattice calculations [7, 8]. This is the case for $m_\sigma = 600$ MeV and $T_0 = 270$ MeV where all three Polyakov loop potentials yield coinciding transitions. This choice also excludes modifications caused by different values of m_σ . Moreover, recent studies [45] point to m_σ -values which lie in the

\mathcal{U}	T_0	m_σ	T_χ	T_χ^s	T_d	$T_\chi \approx T_d$
-	-	800	184	278	-	
-	-	600	146	248	-	
-	-	500	129	238	-	
poly	270	800	228	306	227	*
poly	208	800	204	297	178	
poly	187	800	197	295	161	
poly	178	800	194	273	154	
poly	270	600	204	262	204	*
poly	208	600	179	270	179	*
poly	187	600	171	267	171	*
poly	178	600	166	236	166	*
poly	270	500	193	254	220	
poly	208	500	168	239	168	*
poly	187	500	159	237	159	*
poly	178	500	156	236	156	*
log	270	800	228	302	208	
log	208	800	208	293	166	
log	187	800	204	251	150	
log	270	600	207	274	207	*
log	208	600	180	286	165	
log	187	600	172	283	150	
log	270	500	198	264	198	*
log	208	500	168	255	168	*
log	187	500	159	252	150	
Fuku	-	800	214	289	193	
Fuku	-	600	189	260	189	*
Fuku	-	500	179	250	179	*

TABLE II: The (pseudo)critical temperatures of the chiral transition for the light (T_χ), strange (T_χ^s) and the deconfinement transition (T_d) at $\mu_q = 0$ for different m_σ and Polyakov loop potentials in units of MeV, evaluated for physical pion masses. In the last column the coincidence of the chiral and deconfinement transition is labeled with *.

lower range of the broad experimental σ -resonance region (400 MeV...1200 MeV) [44].

For a proper comparison of the model results with the HotQCD [8] and RBC-Bielefeld lattice data [7, 31, 32], we also adjust the pion masses accordingly. We denote the mass values of $m_K = 503$ MeV and $m_\pi = 220$ MeV which are used in lattice simulations as ‘lattice point’ and the measured values of $m_K = 495$ MeV and $m_\pi = 138$ MeV as the ‘physical point’. In the model calculation the tuning of the meson masses is achieved by adjusting the explicit symmetry breaking parameters h_x and h_y accordingly. Heavier meson masses yield also slightly heavier constituent quark masses

$$m_l \approx 322 \text{ MeV (300 MeV)}, \quad m_s \approx 438 \text{ MeV (433 MeV)}$$

where the values in parentheses are obtained at the physical point.

The increased meson masses shift the transition to higher temperatures, see Tab. III. The strongest shift is seen in the non-strange chiral transition since the change of the light quark masses is larger than that of the strange quark mass in this sector. Both, the non-strange and the deconfinement transition still coincide. The strange

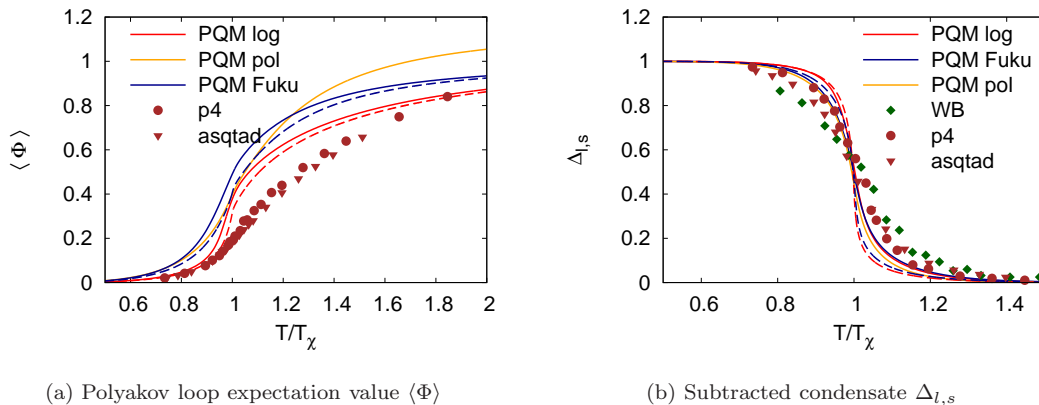


FIG. 1: (color online) The Polyakov loop expectation value $\langle \Phi \rangle$ (left panel) and the subtracted condensate $\Delta_{l,s}$ (right panel) as a function of temperature for different Polyakov loop potentials in comparison to lattice data of the HotQCD (p4 and asqtad, $N_\tau = 8$) [8] and Wuppertal-Budapest collaborations (WB, $N_\tau = 10$, $m_\pi = 135$ MeV) [10]. Solid lines correspond to larger pion and kaon masses as used in the HotQCD simulations, dashed lines to physical masses.

quark sector is almost unaffected.

In Fig. 1(a) the Polyakov loop expectation value $\langle \Phi \rangle$ is shown as a function of temperature for three different Polyakov loop potentials. The solid lines correspond to heavier meson masses evaluated at the lattice point and the dashed lines to the physical ones. The expectation values are slightly larger for Fukushima's potential than for the logarithmic potential which exhibits a sharper crossover. The influence of the higher meson masses is mild. The observed shift may be explained by the larger T_χ/T_0 ratio for heavier pion masses. The lattice data show a rather smooth transition with significant lower values for the Polyakov loop expectation value. For clarity we omit the error bars of the lattice data here and in the following figures.

The sharper transition in the model as well as the higher values of the Polyakov loop are probably a remnant of the construction of the Polyakov loop potentials in the pure gauge sector, where a strong first order transition is obtained at $T \sim 270$ MeV. In the broken phase, the logarithmic potential comes closest to the lattice data, while the difference between the model results and the lattice is considerable in the restored phase for all potentials.

Only for the polynomial potential the expectation value increases above unity which hampers its interpretation as an order parameter, related to the free energy of a static color charge. However, these findings are in

\mathcal{U}	T_0	m_σ	T_χ	T_χ^s	T_d	$T_\chi \approx T_d$
-	-	600	164	250	-	
poly	270	600	216	263	215	*
log	270	600	215	275	208	*
Fuku	-	600	200	261	196	*

TABLE III: Pseudocritical temperatures similar to Tab. II but for $m_\pi = 220$ MeV. See text for details.

agreement with other model studies for three quark flavors, e.g. [24, 30]. In a previous two-flavor PQM study $\langle \Phi \rangle > 1$ was only observed at non-vanishing chemical potential [36]. For the other Polyakov loop potentials the logarithmic divergence avoids expectation values larger than one.

In contrast to the Polyakov loop expectation value, a comparison of the chiral order parameter $\langle \bar{q}q \rangle$ is more involved since some renormalization/normalization factors are unknown. Thus, a more suitable quantity, to compare with, is the ratio

$$\Delta_{l,s} = \frac{\langle \bar{l}l \rangle(T) - (\hat{m}_l/\hat{m}_s)\langle \bar{s}s \rangle(T)}{\langle \bar{l}l \rangle(0) - (\hat{m}_l/\hat{m}_s)\langle \bar{s}s \rangle(0)} \quad (24)$$

which includes the non-strange $\langle \bar{l}l \rangle$ and strange $\langle \bar{s}s \rangle$ condensate. This corresponds to

$$\Delta_{l,s} = \frac{\langle \sigma_x \rangle(T) - (h_x/h_y)\langle \sigma_y \rangle(T)}{\langle \sigma_x \rangle(0) - (h_x/h_y)\langle \sigma_y \rangle(0)} \quad (25)$$

in our model calculation, where the quark condensates have been replaced by $\langle \sigma_x \rangle$ and $\langle \sigma_y \rangle$ accordingly. Since the bare quark masses \hat{m}_l, \hat{m}_s are not directly available, the ratio of the explicit symmetry breaking parameters $h_{x,y}$ is used instead. They are proportional to the bare quark masses up to a constant that drops out in the ratio, see e.g. [1].

In Fig. 1(b) the results for the subtracted condensate $\Delta_{l,s}$ are shown. The model calculations for $\Delta_{l,s}$ are in better agreement with the lattice data than the ones for the Polyakov loop expectation value. The lattice data exhibit a somewhat smoother transition than the model results. The logarithmic Polyakov loop potential generates the sharpest transition while Fukushima's and the polynomial potential are closer to the lattice results. The influence of the larger meson masses is more pronounced in the broken phase, where the transition becomes smoother

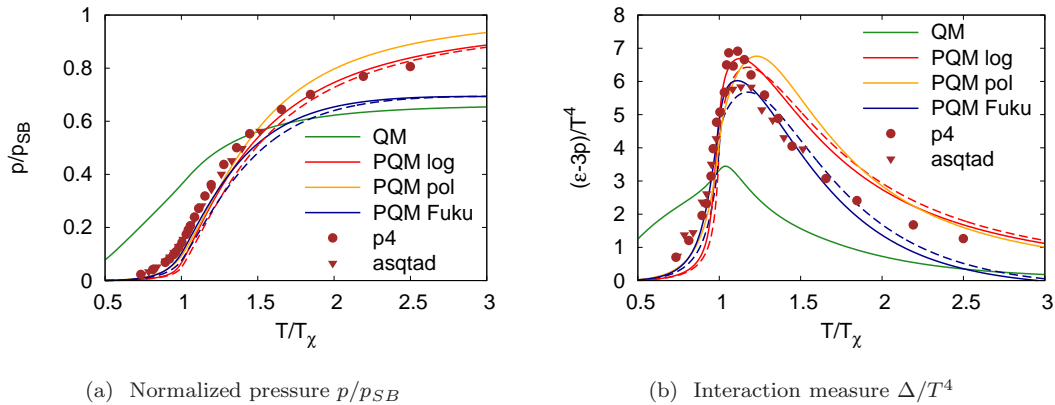


FIG. 2: (color online) The normalized pressure (left panel) and the interaction measure (right panel) as a function of temperature. The model calculations (PQM model with various Polyakov loop potentials and the QM model) are compared to lattice data ($N_\tau = 8$, p4 and asqtad actions) from [8]. Solid lines correspond to larger pion and kaon masses as used in the lattice simulations, dashed lines to physical masses.

for larger meson masses. The data of the Wuppertal-Budapest group suggest a much smoother transition. This effect is enhanced in the figure due to the transition temperature normalization. The transition temperature is much smaller in the Wuppertal-Budapest simulation than for the model or HotQCD simulations. Since the Wuppertal-Budapest data are obtained for physical quark masses they have to be compared to the dashed model curves which suggest an even sharper transition than the ones obtained for heavier pion masses.

V. QCD THERMODYNAMICS

In order to address the modifications of the Polyakov loop on the equilibrium thermodynamics we evaluate several thermodynamic quantities and compare the PQM model analysis with the QM model without the Polyakov loop and recent QCD lattice simulations. The bulk thermodynamic observables such as pressure, energy and entropy density are sensitive to the change from hadronic to quark-gluon degrees of freedom and thus reflect some deconfining aspects of a QCD phase transition.

Pressure

The pressure is obtained directly from the grand potential via

$$p(T, \mu_q) = -\Omega(T, \mu_q) \quad (26)$$

with the vacuum normalization $p(0, 0) = 0$. In the model calculations it is the primary observable and other thermodynamic quantities can be obtained from it by differentiation. Note that this procedure differs from the lattice approach, where for convenience the trace of the energy-momentum tensor Θ_μ^μ is taken as the basis for the

thermodynamic observables evaluation [8]. For example, the pressure is then obtained by integration over the trace of the energy-momentum tensor Θ_μ^μ [46]

$$p(T) = p(T_i) + \int_{T_i}^T dT' \frac{1}{T'^5} \Theta_\mu^\mu \quad (27)$$

with the integration constant $p(T_i)$. In order to make the constant as small as possible the temperature T_i is adjusted accordingly, e.g., $T_i \sim 100$ MeV [47] and $p(T_i)$ is finally dropped. The suppression of this constant corresponds to an approximation in the lattice data.

Another normalization of the pressure lattice data consists in applying the pressure from the hadron resonance gas (HRG), $p_{HRG}(T_i)$, which provides a realistic description of the pressure in the chirally broken phase.

Since $p_{HRG}(T_i = 100 \text{ MeV})/T_i^4 \sim 0.8$ [8] this normalization shifts the lattice data to slightly higher values.

In Fig. 2(a) the pressure for the PQM and QM models, normalized to the Stefan-Boltzmann limit (SB) of the PQM model, is compared to lattice data. Explicitly, the pressure of $N_c^2 - 1$ massless gluonic and of N_f massless fermionic degrees of freedom tends to

$$\frac{p_{SB}}{T^4} = (N_c^2 - 1) \frac{\pi^2}{45} + N_c N_f \frac{7\pi^2}{180}, \quad (28)$$

at high temperature, which we use for normalization. Of course, no gluons are involved in the pure QM model and consequently, the first term in Eq. (28) does not contribute. Therefore, a lower pressure is obtained in the QM model for high temperatures in the figure. The same conclusion holds for the PQM with Fukushima's potential.

As expected, the QM model fails in describing the lattice data for all temperatures, while all PQM model results are in reasonable agreement with the data. The best agreement around T_χ with the lattice data is achieved with Fukushima's potential but it fails for temperatures

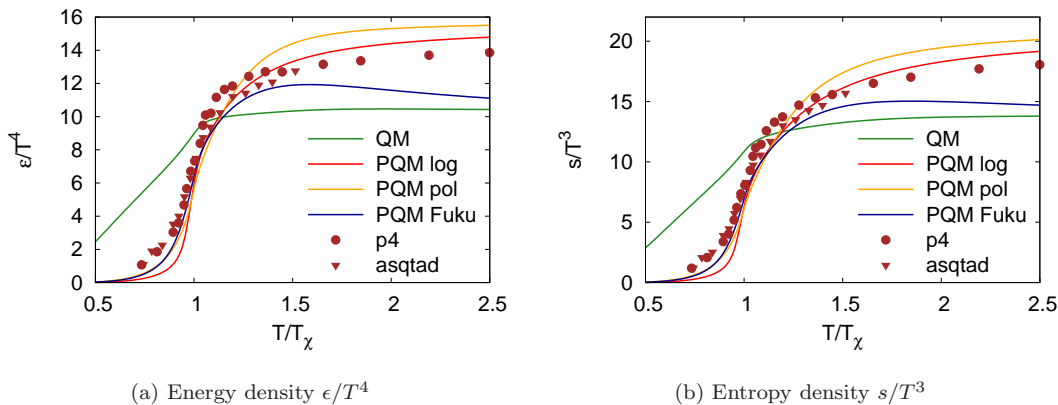


FIG. 3: (color online) The energy- (left panel) and entropy density (right panel) similar to Fig. 2.

above $1.5T_\chi$ as already discussed in Sec. II A. Note that for the HotQCD lattice data the transition temperature lies between $T_\chi \approx 185 - 195$ MeV. We have used the average value $T_\chi = 190$ MeV in the figures. Physical meson masses reduce the pressure in particular around T_χ (dashed lines in Fig. 2(a)).

The better agreement of the pressure of Polyakov-loop augmented chiral models with lattice data has already been observed in two-flavor studies such as in [36] for the PQM and in [13] for the PNJL model. However, these model findings, obtained for physical pion masses, are compared with lattice data for two rather heavy quark flavors [22]. To some extent, the agreement is therefore fortuitous since, on the one hand, mesonic fluctuations are more suppressed in lattice simulations if heavier masses are applied and, on the other hand, mean-field approximations do not consider fluctuations around the mean-fields. In this work larger pion masses are taken into account for the lattice comparison.

Interaction measure, energy density and entropy density

The interaction measure $\Delta = e - 3p$ is related to the grand potential via a temperature derivative

$$\frac{\Delta}{T^4} = T \frac{\partial}{\partial T} \left(\frac{p}{T^4} \right) = -T \frac{\partial}{\partial T} \left(\frac{\Omega}{T^4} \right) \quad (29)$$

and can be obtained directly in lattice simulations from the trace of the energy-momentum tensor

$$\frac{\Theta_\mu^\mu}{T^4} = \frac{\epsilon - 3p}{T^4} = \frac{\Delta}{T^4}. \quad (30)$$

In the interaction measure finite volume and discretization effects are more apparent than, e.g., in the pressure (c.f. [8]).

In Fig. 2(b) the model calculations for the interaction measure are compared to $N_\tau = 8$ lattice data. The height of the peak in the lattice simulations depends significantly on the lattice size as well as on the lattice action.

Away from the phase transition the volume dependence is less pronounced [8]. In the chirally broken phase, the lattice data are close to all model curves. Around the transition at $T \approx T_\chi$ Fukushima's potential is closest to the asqtad-action data, while the remaining two model curves are in better agreement with the p4-action data. In general, the peak height decreases on larger lattices and in particular for the p4-action. For these temperatures the asqtad-action shows a weak N_τ -dependence [8]. In contrast to the pressure, the logarithmic and polynomial Polyakov model version cannot describe the lattice data in the symmetric phase while Fukushima's ansatz approaches the data at least up to $T \sim 1.5T_\chi$.

In a PNJL study similar findings are obtained in the broken phase, but a more rapid decrease is seen in the restored phase [25]. For physical pion masses, the interaction measure and the height of the maximum decreases for temperatures below the transition. Above the transition the interaction measure increases for smaller pion masses.

To complete the thermodynamic comparison we also show the energy density ϵ and the entropy density s , defined as

$$\epsilon = -p + Ts \quad , \quad s = -\frac{\partial \Omega}{\partial T}, \quad (31)$$

in Fig. 3 as a function of temperature. The rapid increase of the energy density signals the liberation of light quark degrees of freedom. It increases almost to the value of an ideal gas of massless quarks and gluons.

Speed of sound c_s and specific heat cv

For hydrodynamical investigations of relativistic heavy-ion collisions the speed of sound c_s is an important quantity. Its square at constant entropy is defined by

$$c_s^2 = \frac{\partial p}{\partial \epsilon} \Big|_S = \frac{\partial p}{\partial T} \Big|_V \Big/ \frac{\partial \epsilon}{\partial T} \Big|_V = \frac{s}{c_V}, \quad (32)$$

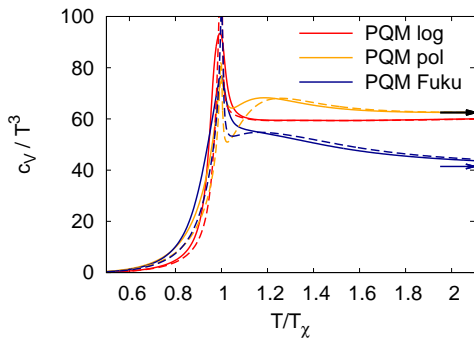
(a) Specific heat capacity c_V/T^3

FIG. 4: (color online) The specific heat capacity in the PQM model as a function of temperature. Solid lines have been obtained for $m_\pi = 220$ MeV, dashed lines for physical values. The arrows indicate the SB-limit. See text for details.

where

$$c_V = \left. \frac{\partial \epsilon}{\partial T} \right|_V = -T \left. \frac{\partial^2 \Omega}{\partial T^2} \right|_V \quad (33)$$

denotes the specific heat capacity at constant volume. At a second-order phase transition, where the specific heat diverges with the critical exponent α , the sound velocity drops to zero since the entropy density stays finite, see e.g. [48] for a two-flavor QM model calculation.

The specific heat calculated in the three-flavor PQM model at $\mu_q = 0$ as a function of the temperature is displayed in Fig. 4(a) for three different Polyakov loop potentials. The solid lines in this figure correspond to masses used in lattice simulations and the dashed lines to physical masses. The specific heat grows with increasing temperatures, peaks at the transition temperature and approaches the corresponding SB-limit for high temperatures. The SB limits deviate due to the differences in the contributing gluon degrees of freedom. For Fukushima's potentials the first term in Eq. (28) is neglected. For smaller masses the peak is sharper. Just after the peak a broad bump around $1.2 T/T_\chi$ is found for the polynomial and Fukushima's potential (for the latter with physical masses). Then c_V goes gradually to the ideal gas value from above.

The velocity of sound as well as the ratio p/ϵ are shown in Fig. 5 as a function of temperature (left panel) and $\epsilon^{1/4}$ (right panel). The latter plot eliminates uncertainties due to the normalization of the transition temperature. For all models including the pure QM model c_s^2 approaches the ideal gas value of $1/3$ at high temperatures of about $2.5T_c$ and can well be approximated by the ratio p/ϵ . Furthermore, the value of p/ϵ matches with the one of c_s^2 for low temperatures. In between these two limits c_s^2 is always larger than p/ϵ except near T_χ , similar as in a two-flavor PNJL analysis [15].

Near T_χ it drops to a minimum of about 0.04 for the PQM model, whereas the minimum is close to 0.16 if the

Polyakov loop is neglected. While the latter value 0.16 is close to the results for pure YM theory on the lattice [49] we find a minimum including the Polyakov loop almost half of the softest point $P/\epsilon = 0.075$ in [50] for two-flavor staggered fermions. It is interesting that in our work even at temperatures around $0.5T_\chi$ c_s^2 is not larger than 0.1 if the Polyakov loop is included. This is in contrast to Ref. [51] where a confinement model has been used and values of about $c_s^2 \sim 0.2$ around $0.5T_\chi$ and $c_s^2 = 0.15$ around T_χ are found which correspond to our values for the pure QM model.

Since the speed of sound is related to the interaction measure via

$$\frac{\Delta}{\epsilon} = \frac{\epsilon - 3p}{\epsilon} \approx 1 - 3c_s^2, \quad (34)$$

a minimum in the speed of sound as expected near a phase transition translates to a maximum in the conformal measure Δ/ϵ . For high temperatures where c_s^2 reaches the SB limit of $1/3$ the conformal measure should vanish.

In the left panel of Fig. 5 where both quantities c_s^2 and p/ϵ are shown as a function of $\epsilon^{1/4}$ the best agreement with the lattice data is achieved with Fukushima's potential model.

Quark number susceptibilities and Kurtosis

Quark number susceptibilities incorporate information on thermal fluctuations of the degrees of freedom that carry a net number of light or strange quarks. They are also related to the second order cumulant of an expansion in the net quark number $\delta n_q = n_q - \langle n_q \rangle$, e.g. [52].

In the transition region these susceptibilities changes because the carriers of charge, strangeness or baryon number are heavy hadrons in the low temperature phase but much lighter quarks at high temperatures. Thus, at low temperatures they describe the fluctuations of hadrons carrying net light quark or strangeness quantum numbers. For example, the light quark number susceptibility, χ_l , receives basically only contributions from the lightest hadrons, the pions, at low temperatures, i.e. $\chi_l/T^2 \propto \exp(-m_\pi/T)$ where the index l refers to the light quark flavors. Correspondingly, χ_s/T^2 receives contributions only from the lightest hadron that carries strangeness. For high temperatures and N_f quark flavors these susceptibilities approach the SB value for an ideal massless quark gas with N_c colors, i.e. $\chi_q/T^2 \rightarrow N_f N_c/3$.

Furthermore, the quark number susceptibility χ_q corresponds to the first Taylor coefficient c_2 of an expansion of the thermodynamic pressure in powers of μ_q/T

$$\frac{p}{T^4} = \sum_{n=0}^{\infty} c_n(T) \left(\frac{\mu_q}{T} \right)^n \quad \text{with} \quad c_n(T) = \left. \frac{1}{n!} \frac{\partial^n (p/T^4)}{\partial (\mu_q/T)^n} \right|_{\mu_q=0}. \quad (35)$$

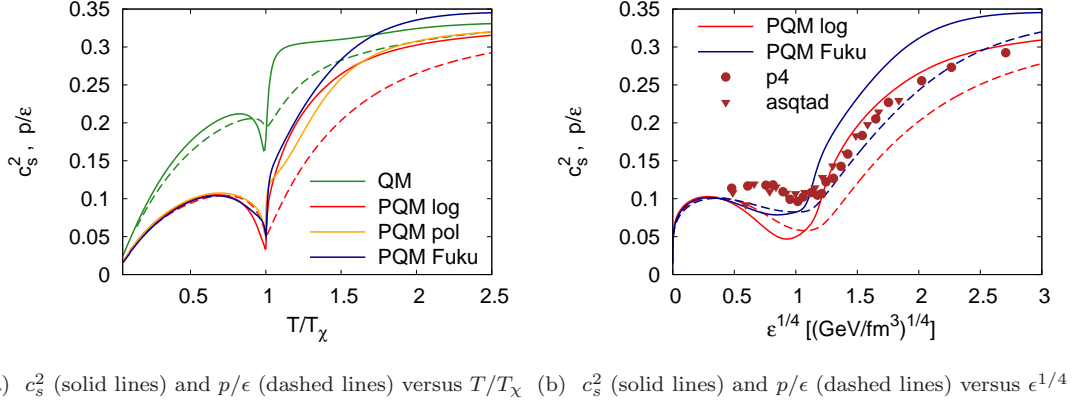


FIG. 5: (color online) Left panel: The squared speed of sound c_s^2 (solid lines) and the ratio p/ϵ (dashed lines) as a function of temperature. Right panel: For comparison with lattice data (p/ϵ from [8]) both quantities are also shown as a function of $\epsilon^{1/4}$.

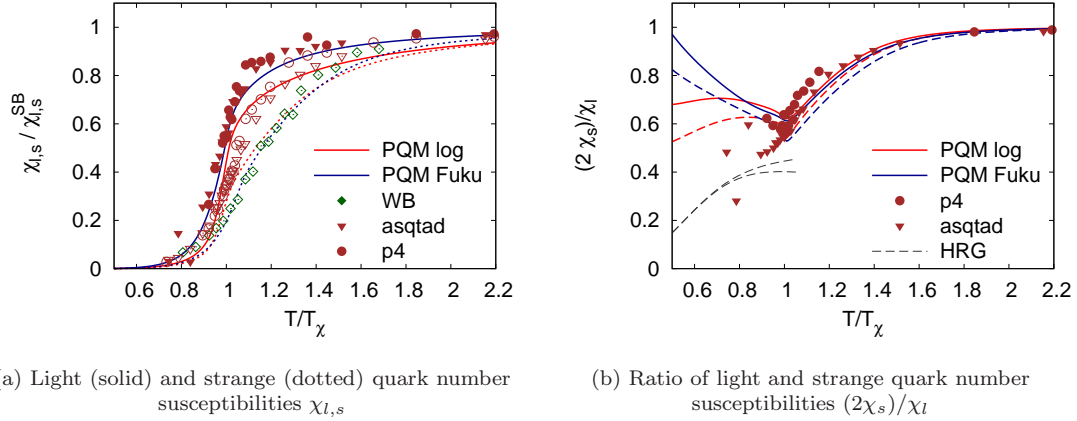


FIG. 6: (color online) Left panel: The light (solid lines/filled symbols) and strange (dotted lines/open symbols) quark number susceptibilities in comparison with lattice data ($N_\tau = 8$) with larger lattice pion and kaon masses [8]. For χ_s we also show results of the Wuppertal-Budapest group (WB) obtained with physical pion masses on $N_\tau = 10$ lattices [10]. Right panel: The ratio of the strange and light quark number susceptibilities with physical meson masses (dashed lines) and lattice masses (solid lines) in comparison with lattice data. Also shown are the results for a hadron resonance gas model (HRG) including resonances up to 1.5 GeV (upper curve) and 2.5 GeV (lower curve) from [8].

It can be obtained from the grand potential as follows

$$\frac{\chi_q}{T^2} = 2c_2 = \frac{1}{T^3 V} \langle (\delta n_q)^2 \rangle = -\frac{\partial^2 \Omega}{T^2 \partial \mu_q^2}. \quad (36)$$

At a second order transition χ_q diverges and, since the quark number density stays finite, the isothermal compressibility also diverges, see e.g. [53].

In the present (2+1)-flavor analysis we investigate the light and strange quark number susceptibilities separately

$$\chi_l = -\frac{\partial^2 \Omega}{\partial \mu_l^2}, \quad \chi_s = -\frac{\partial^2 \Omega}{\partial \mu_s^2}. \quad (37)$$

The required derivatives of the thermodynamic potential can be calculated with a novel algorithmic differentiation technique, described in [54].

Both susceptibilities, normalized according to their SB limit, are shown in Fig. 6(a). Around the chiral transition temperature the light susceptibility χ_l raises faster than the strange susceptibility. In general, the PQM model results for the susceptibilities are below the lattice data. Closest to the model findings are the Wuppertal-Budapest data for χ_s which have been obtained with physical pion and kaon masses. However, the influence of the pion mass in the strange sector is weak. The better agreement might be related to the larger lattices ($N_\tau = 10$) of the Wuppertal-Budapest group.

To avoid unknown normalization factors in the lattice data (cf. [32]) it is more convenient to consider the ratio of the strange and light quark number susceptibilities as shown in Fig. 6(b). In the restored phase and around the transition the agreement with the lattice data is good. Note that the two different lattice actions devi-

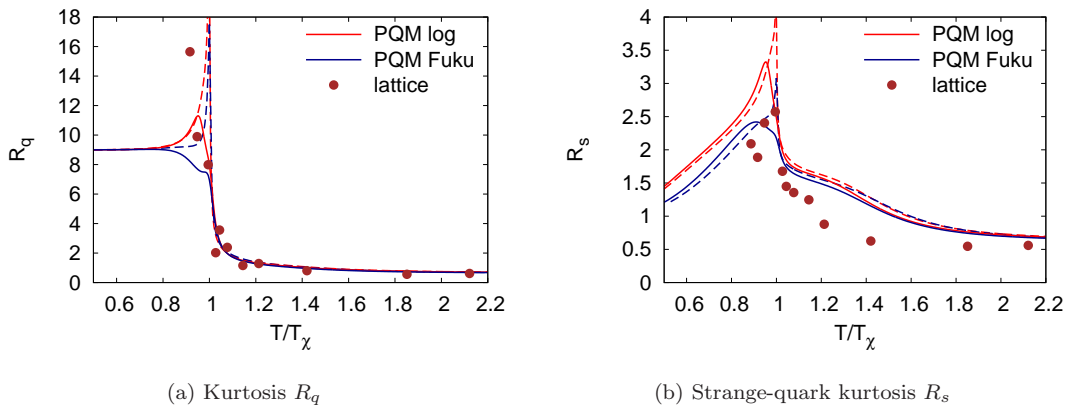


FIG. 7: (color online) Left panel: Kurtosis R_q for uniform quark chemical potentials as a function of temperature. Right panel: Kurtosis R_s for the strange quark sector. The lattice data ($N_\tau = 6$) are taken from [32].

ate strongly.

The ratio of the strange and light susceptibilities (right panel) shows strong deviations of the model calculation from either the lattice data or a HRG model calculation in the broken phase. This might be attributed to the omission of mesonic fluctuations in the mean-field approximation of the PQM model. Since the light and strange fluctuations are mainly driven by the light pions and heavy kaons respectively, this results in rather small ratios for the HRG model calculation whereas values in between 0.5 – 1.0 are found for the PQM model.

Another quantity which probes deconfinement is the kurtosis of the quark number fluctuations R_q . It is defined as the ratio of the fourth derivative of the grand potential with respect to μ_q , i.e. $\chi_{q,4} \equiv -\partial^4 \Omega / \partial \mu_q^4$, and the quark number susceptibility

$$R_q \equiv \frac{T^2 \chi_{q,4}}{\chi_q}. \quad (38)$$

It is sensitive to the net quark content of baryon number carrying effective degrees of freedom. At small temperature, the effective degrees of freedom in the PQM model are three-quark states since the Polyakov loop vanishes there and suppresses the one- and two-quark states in the thermodynamic potential, see Eq. (20). Thus, the quark/antiquark contribution of the thermodynamic potential is basically that of a non-interacting system with particles and antiparticles carrying baryon number $B = \pm 1$. Consequently, the kurtosis tends in the low-temperature confined phase with $|B| = 1$ to $R_q = (N_c B)^2 = 9$. Without the Polyakov loop, e.g. in a pure QM model, the kurtosis would tend to one since in this case single quarks with $|B| = 1/3$ would contribute at all temperatures. Thus, the correct low-temperature value for the kurtosis is obtained only with the Polyakov loop.

At high temperatures the Polyakov loop tends to one, Fig. 1(a). As a consequence, the quark/antiquark contribution of the thermodynamic potential, Eq. (20), corresponds to a system of non-interacting quark gas and

the kurtosis reaches the SB value, $R_q \rightarrow 6/\pi^2$. Both temperature limits of R_q are precisely reproduced with the PQM model as shown in Fig. 7. The kurtosis is almost temperature independent far below and above the transition. But around the transition it is strongly dependent on the meson masses and the effective implementation of the Polyakov loop and its coupling to the quark sector of the model. The PQM model calculation is consistent with lattice data ($N_\tau = 6$) [32]. At the transition the lattice data depict a peak behavior in R_q for larger meson masses ($m_\pi \sim 220$ MeV) but the volume dependence and errors there are still large. As already mentioned, only the PQM model provides the correct low-temperature limit $R_q = 9$ and reaches the high-temperature limit already at $T \sim 1.3T_\chi$ similar to a two-flavor PQM analysis with a polynomial Polyakov loop potential [55]. For Fukushima's potential we observe a similar dependence of the peak structure on the pion mass, i.e., it vanishes for larger masses. The peak structure is more pronounced for a logarithmic potential and survives if the masses are increased. Interestingly, in a three-flavor PNJL analysis with Fukushima's potential no peak is seen even for physical pion masses [25]. A two-flavor PNJL model with a logarithmic potential gives a temperature dependent kurtosis in the broken phase for $T < T_\chi$, which we also find in this work if we consider only the kurtosis for light flavors, i.e., $R_l = T^2 \chi_{l,4} / \chi_l$.

In Fig. 7(b) the kurtosis for the pure strange sector $R_s = T^2 \chi_{s,4} / \chi_s$ is presented. For the lattice simulations $N_\tau = 6$ and physical strange quark masses have been used. Note that chiral symmetry in the strange sector is restored at $T_\chi^s \sim 1.3T_\chi$. For these temperatures the lattice data are already quite close to the SB-limit while the model analysis still yields an enhanced ratio. The strange quark kurtosis rises, and peaks at the chiral symmetry restoration for the light quarks. It stays above the lattice data until the symmetry is fully restored also in the strange sector and drops finally to its SB limit for high temperatures.

VI. SUMMARY

In the present work we have extended a previously introduced two-flavor Polyakov-quark-meson (PQM) model [36] to three quark flavors. This model with the Polyakov loop can address certain confinement issues and is an improvement of the known chiral quark-meson model with three quark flavors. Several aspects, in particular the bulk thermodynamics, of the $(2 + 1)$ -flavor QCD phase transitions are in much better agreement with recent $(2 + 1)$ -flavor lattice simulations.

The Polyakov loop potential is not uniquely determined and different versions are available. Here, we have considered three different effective Polyakov loop potentials which all reproduce a first-order phase transition in the pure gauge sector of the theory at $T_c = 270$ MeV. In two Polyakov potential versions a further parameter T_0 enters which we have varied in order to investigate the influence of finite quark masses on the transition. The scalar and pseudoscalar chiral sector of the PQM model is fitted to the mass spectrum and decay constants in the vacuum. The input masses are experimentally well-known except for the scalar σ -resonance. Different sigma mass values have a strong influence on the chiral phase transition. In this work we have additionally considered various input values for the σ mass similar as in [39].

For some parameter combinations a coincidence of the chiral and deconfinement phase transition at vanishing chemical potential is found which we have used to study the bulk thermodynamics of the finite temperature transition.

The model results are confronted with recent lattice simulations for $2 + 1$ quark flavors of the RBC-Bielefeld [32] and HotQCD [8] collaborations. The latter lattice group uses lattices with temporal extent $N_\tau = 8$ and the quark masses in these simulations are still above the expected physical ones. These quark masses correspond to a kaon mass of $m_K = 503$ MeV and a pion mass of $m_\pi = 220$ MeV. This difference in the masses influences the bulk thermodynamics and its effect is also addressed in this work.

In addition, for the chiral order parameter and the strange quark number susceptibility lattice results for physical quark masses on $N_\tau = 10$ lattices of the Wuppertal-Budapest group [10] are available and compared with the model analysis.

We observe a nice matching with the lattice data for the chiral transition, although the transition is smoother on the lattice, in particularly for the Wuppertal-Budapest results. The lattice data for the Polyakov loop are below the model data, especially in the deconfined phase.

A very good agreement of the lattice data with the model is found for the equation of state in the transition region and for temperatures up to $1.5T_\chi$.

Due to the omission of mesonic fluctuations in the mean-field approximation a deviation of the model and

the lattice data is expected at low temperatures. Similarly, at high temperatures, the gluon dynamics is not fully addressed in the model which may also cause further deviation.

The pressure is not very sensitive to different implementations of the Polyakov loop potential and to details of the lattice simulations. This is in contrast to the interaction measure where Fukushima's potential describes best the lattice data in this temperature regime, especially, with regard to the asqtad-action.

For higher derivatives of the thermodynamic potential such as the quark-number susceptibilities the picture changes. The model results are always below the lattice data. This is the case not only in the chirally broken phase which is understandable due to the omission of mesonic fluctuations but also in the symmetric phase.

Furthermore, there are also some normalization factors involved in the lattice data as well as some volume dependence. For example, the susceptibilities decrease from $N_\tau = 4$ to $N_\tau = 8$ lattices. Interestingly, the $N_\tau = 10$ data for χ_s of the Wuppertal-Budapest group are very close to our model results. However, the normalization factors drop out in the ratio χ_s/χ_l . As a consequence the model results come closer to the lattice in the symmetric phase. In the broken phase the PQM model is far off the lattice and HRG results which might be an artifact of the mean-field approximation.

In summary, we found that the PQM model gives a reasonable description of the bulk thermodynamics in the QCD transition region. The current implementation of the Polyakov loop into the chiral quark-meson model is certainly an improvement but still further developments are required. It seems that the remnant of the first-order transition in the pure gauge sector modifies the chiral and deconfinement transition at finite quark masses such that the transition becomes much sharper compared to lattice data. The sudden liberation of the fermionic degrees of freedom in the model triggers this sharp behavior. This might change if one goes beyond the mean-field approximation. In this case the mesonic fluctuations also contribute to the thermodynamics and drive the phase transition.

Acknowledgments

We thank F. Karsch, C. Schmidt and Z. Fodor for providing lattice data and discussions. The work of MW was supported by the Alliance Program of the Helmholtz Association (HA216/EMMI) and BMBF grants 06DA123 and 06DA9047I. JW was supported in part by the Helmholtz International Center for FAIR. We further acknowledge the support of the European Community-Research Infrastructure Integrating Activity Study of Strongly Interacting Matter under the Seventh Framework Programme of EU.

-
- [1] H. Meyer-Ortmanns, *Rev. Mod. Phys.* **68**, 473 (1996).
- [2] D. H. Rischke, *Prog. Part. Nucl. Phys.* **52**, 197 (2004).
- [3] P. F. Kolb and U. W. Heinz, in *Quark-Gluon Plasma 3*, edited by R. C. Hwa and X.-N. Wang (World Scientific, Singapore, 2004), p. 634.
- [4] F. Karsch, *Lect. Notes Phys.* **583**, 209 (2002); O. Philipsen, *Eur. Phys. J. Spec. Top.* **152**, 29 (2007).
- [5] Y. Aoki, G. Endrodi, Z. Fodor, S. D. Katz, and K. K. Szabo, *Nature* **443**, 675 (2006).
- [6] F. Karsch and M. Lutgemeier, *Nucl. Phys.* **B550**, 449 (1999).
- [7] M. Cheng et al., *Phys. Rev.* **D74**, 054507 (2006).
- [8] A. Bazavov et al., *Phys. Rev.* **D80**, 014504 (2009).
- [9] Y. Aoki, Z. Fodor, S. D. Katz, and K. K. Szabo, *Phys. Lett.* **B643**, 46 (2006).
- [10] Y. Aoki et al., *JHEP* **06**, 088 (2009).
- [11] R. D. Pisarski and F. Wilczek, *Phys. Rev.* **D29**, 338 (1984).
- [12] E. Megias, E. Ruiz Arriola, and L. L. Salcedo, *Phys. Rev.* **D74**, 065005 (2006); E. Megias, E. Ruiz Arriola, and L. L. Salcedo, *Phys. Rev.* **D74**, 114014 (2006).
- [13] C. Ratti, M. A. Thaler, and W. Weise, *Phys. Rev.* **D73**, 014019 (2006).
- [14] S. Roessner, C. Ratti, and W. Weise, *Phys. Rev.* **D75**, 034007 (2007).
- [15] S. K. Ghosh, T. K. Mukherjee, M. G. Mustafa, and R. Ray, *Phys. Rev.* **D73**, 114007 (2006).
- [16] C. Sasaki, B. Friman, and K. Redlich, *Phys. Rev.* **D75**, 074013 (2007).
- [17] S. Roessner, T. Hell, C. Ratti, and W. Weise, *Nucl. Phys.* **A814**, 118 (2007).
- [18] D. Blaschke, M. Buballa, A. E. Radzhabov, and M. K. Volkov, *Yadernaya Fizika*, vol. 71, no. **11**, 2012 (2008).
- [19] T. Hell, S. Roessner, M. Cristoforetti, and W. Weise, *Phys. Rev.* **D79**, 014022 (2008).
- [20] H. Abuki, R. Anglani, R. Gatto, G. Nardulli, and M. Ruggieri, *Phys. Rev.* **D78**, 034034 (2008).
- [21] J. Steinheimer, S. Schramm, and H. Stöcker, [arXiv:0909.4421](https://arxiv.org/abs/0909.4421) [[hep-ph](https://arxiv.org/abs/0909.4421)].
- [22] A. Ali Khan et al. (CP-PACS), *Phys. Rev.* **D64**, 074510 (2001).
- [23] M. Ciminale, R. Gatto, N. D. Ippolito, G. Nardulli, and M. Ruggieri, *Phys. Rev.* **D77**, 054023 (2007).
- [24] W.-J. Fu, Z. Zhang, and Y.-X. Liu, *Phys. Rev.* **D77**, 014006 (2007).
- [25] K. Fukushima, *Phys. Rev.* **D77**, 114028 (2008).
- [26] K. Fukushima, *Phys. Rev.* **D78**, 114019 (2008).
- [27] K. Fukushima, *Phys. Rev.* **D79**, 074015 (2009).
- [28] B.-J. Schaefer and M. Wagner, *Progress in Particle and Nuclear Physics* **62**, 381 (2009).
- [29] B.-J. Schaefer, M. Wagner, and J. Wambach, *PoS CPOD2009*, 017 (2009).
- [30] H. Mao, J. Jin, and M. Huang, *J. Phys.* **G37**, 035001 (2009).
- [31] M. Cheng et al., *Phys. Rev.* **D77**, 014511 (2008).
- [32] M. Cheng et al., *Phys. Rev.* **D79**, 074505 (2008).
- [33] C. Bernard et al., *Phys. Rev.* **D75**, 094505 (2007).
- [34] Y. Aoki, Z. Fodor, S. D. Katz, and K. K. Szabo, *JHEP* **01**, 089 (2006).
- [35] J. Braun, L. M. Haas, F. Marhauser, and J. M. Pawłowski, [arXiv:0908.0008](https://arxiv.org/abs/0908.0008) [[hep-ph](https://arxiv.org/abs/0908.0008)].
- [36] B.-J. Schaefer, J. M. Pawłowski, and J. Wambach, *Phys. Rev.* **D76**, 074023 (2007).
- [37] M. Gell-Mann and M. Levy, *Nuovo Cim.* **16**, 705 (1960).
- [38] A. M. Polyakov, *Phys. Lett.* **B72**, 477 (1978).
- [39] B.-J. Schaefer and M. Wagner, *Phys. Rev.* **D79**, 014018 (2009).
- [40] R. D. Pisarski, *Phys. Rev.* **D62**, 111501 (2000).
- [41] A. Dumitru and R. D. Pisarski, *Phys. Lett.* **B525**, 95 (2002).
- [42] C. Ratti and W. Weise, *Phys. Rev.* **D70**, 054013 (2004); C. Ratti, S. Roessner, and W. Weise, *Phys. Lett.* **B649**, 57 (2007).
- [43] J. Braun and H. Gies, *Phys. Lett.* **B645**, 53 (2005); J. Braun and H. Gies, *JHEP* **06**, 024 (2006).
- [44] W. M. Yao et al. (Particle Data Group), *J. Phys.* **G33**, 1 (2006).
- [45] I. Caprini, G. Colangelo, and H. Leutwyler, *Phys. Rev. Lett.* **96**, 132001 (2006); F. J. Yndurain, R. Garcia-Martin, and J. R. Pelaez, *Phys. Rev.* **D76**, 074034 (2007).
- [46] F. Karsch and E. Laermann, [arXiv:hep-lat/0305025](https://arxiv.org/abs/hep-lat/0305025).
- [47] F. Karsch, *PoS CPOD07*, 026 (2007).
- [48] B.-J. Schaefer and H.-J. Pirner, *Nucl. Phys.* **A660**, 439 (1999).
- [49] R. V. Gavai, S. Gupta, and S. Mukherjee, *Pramana* **71**, 487 (2008).
- [50] S. Ejiri, F. Karsch, E. Laermann, and C. Schmidt, *Phys. Rev.* **D73**, 054506 (2006).
- [51] B. Mohanty and J.-E. Alam, *Phys. Rev.* **C68**, 064903 (2003).
- [52] M. A. Stephanov, *Phys. Rev. Lett.* **102**, 032301 (2009).
- [53] B.-J. Schaefer and J. Wambach, *Phys. Rev.* **D75**, 085015 (2007).
- [54] M. Wagner, A. Walther, and B.-J. Schaefer, *Comp. Phys. Commun.* **181**, 756 (2010).
- [55] B. Stokic, B. Friman, and K. Redlich, *Phys. Lett.* **B673**, 192 (2008).